POLITECNICO DI TORINO
Repository ISTITUZIONALE

Plate elements with node dependent kinematics and arbitrary displacement fields for free edge analysis

Original
Plate elements with node dependent kinematics and arbitrary displacement fields for free edge analysis / Carrera, E., Scano, D., Zappino, E.. - In: COMPOSITE STRUCTURES. - ISSN 0263-8223. - 393:(2026). [10.1016/j.compstruct.2026.120633]

Availability:
This version is available at: 11583/3014695 since: 2026-08-20T15:38:33Z

Publisher:
Elsevier

Published
DOI:10.1016/j.compstruct.2026.120633

Terms of use:

This article is made available under terms and conditions as specified in the corresponding bibliographic description in the repository

Publisher copyright

(Article begins on next page)

26 November 2026

Composite Structures 393 (2026) 120633

Contents lists available at ScienceDirect

Composite Structures

journal homepage: www.elsevier.com/locate/compstruct

Plate elements with node dependent kinematics and arbitrary displacement fields for free edge analysis

Erasmo Carrera [*,1], Daniele Scano [2], Enrico Zappino [3]

MUL² Lab, Department of Mechanical and Aerospace Engineering, Politecnico di Torino, Corso Duca degli Abruzzi 24, 10129 Torino, Italy

ARTICLE INFO

Keywords:
Finite element method
Higher-order theories
Kinematic models
Unified Formulation
Node-Dependent Kinematics
Free-edge

ABSTRACT

This paper presents enhanced two-dimensional finite elements based on the Node-Dependent Kinematics approach, in which each finite element node may employ a distinct thickness expansion, while kinematic models can be independently selected for each displacement variable using both Taylor- and Lagrange-based expansions over the thickness. The formulation, developed within the Carrera Unified Formulation, permits the generation of generic structural theories in the same framework. The present method is validated by studying the free-edge problem and comparing results with literature data and high-fidelity reference solutions. The results confirm that the optimal computational model for balancing accuracy and efficiency depends on the specific problem under consideration.

1. Introduction

Laminated composite structures are widely used in aerospace and automotive applications due to their superior strength-to-weight ratio and performance. Their inherent material inhomogeneity, however, can lead to complex mechanical behaviours, such as free-edge effects. These phenomena are localized stress concentrations at layer interfaces near geometric discontinuities. These stress concentrations are critical as they frequently act as initiation points for delamination and other damage mechanisms [1]. See also the influential comprehensive review given by Mittelstedt and Becker [2].

This paper adopts two-dimensional (2D) structural models. Comprehensive reviews of these theories are provided by Reddy [1] and Carrera [3]. The foundational Kirchhoff–Love theory [4,5] represents one of the earliest 2D formulations. The extension to laminated composites, known as Classical Lamination Theory (CLT) [6], assumes that normal surfaces to the mid-plane remain straight and perpendicular during the deformation. The First-Order Shear Deformation Theory (FSDT), proposed in the works of Reissner [7] and Mindlin [8], updates the CLT allowing for transverse shear deformations. Advances in two-dimensional theory, have improved the accuracy of stress analysis by overcoming classical limitations. Comprehensive treatments of these developments are provided in the seminal works [9,10], which establish fundamental theoretical frameworks. Notable contributions include the complete third-order theory by Kant and Manjunatha [11]. Additionally, Reddy [12] and Senthilnathan et al. [13] used a higher-order model that satisfies surface stress conditions. The Equivalent Single-Layer (ESL) approach is commonly adopted in the literature due to its modelling simplicity, as it utilizes kinematic variables that are independent of the number of material layers. For higher-fidelity stress analysis, the Layer-Wise (LW) approach is needed. This method assigns separate variables to each layer, enabling more accurate through-thickness resolution at increased computational expense. See the review by Maji and Mahato [14].

Carrera and colleagues proposed an innovative unified framework model, known as the Carrera Unified Formulation (CUF). Detailed expositions can be found in the book by Carrera et al. [15] and in foundational works such as [3,16]. A key feature of CUF is that its governing equations are invariant, that is, they have the same mathematical structure for every structural theory. The previous high-fidelity models successfully capture complex structural behaviour, but the conventional approaches require costly reformulation for each new theory. Unified frameworks, such as the CUF, erase this limitation by enabling flexible integration of diverse models within a single theoretical framework. Demasi and coworkers [17–19] proposed a novel extension of the CUF, denoted as the Generalized Unified Formulation (GUF), in which the expansion type and kinematic approach can be independently chosen for each displacement component. In these contributions, both strong and weak formulations were developed, with Legendre and Taylor polynomials employed as expansions functions along the thickness.

* Corresponding author.
E-mail addresses: erasmo.carrera@polito.it (E. Carrera), daniele.scano@polito.it (D. Scano), enrico.zappino@polito.it (E. Zappino).
[1] Professor of Aeronautics and Astronautics.
[2] Postdoc Researcher.
[3] Associate Professor.

https://doi.org/10.1016/j.compstruct.2026.120633
Received 18 March 2026; Received in revised form 16 June 2026; Accepted 2 July 2026
Available online 8 July 2026
0263-8223/© 2026 The Authors. Published by Elsevier Ltd. This is an open access article under the CC BY license (http://creativecommons.org/licenses/by/4.0/).

Current methods, however, often cannot assess the individual contributions of kinematic expansion terms and use ESL and LW together. To handle this limitation, Carrera and co-workers [20,21] introduced a novel consistent formulation based on the CUF and GUF principles for the plate and shell formulations. This approach enables users to adaptively select the precision of the kinematic theory and optimize the balance between computational efficiency and predictive accuracy. Recently, Carrera and collaborators [22,23] studied the influence of the terms by using the Asymptotic-Axiomatic Method and created graphs that correlated the error and the number of terms. These concepts, however, trace back to the work of Carrera [24] concerning the multilayered plates. In [25], the influence of the terms in transverse displacement component was studied in shell analyses.

Thus far, expansions have been based primarily on either Taylor or Lagrange expansions. Taylor polynomials may be efficiently adopted to build complicated structural theories in the analysis of 2D structures. These polynomial terms have the form z^p, where p is a positive integer. Carrera and collaborators [26,27] extensively utilized these polynomials in various studies. One of the key advantages of these models is their flexibility, allowing the inclusion of a random number of terms to explore complex phenomena in greater detail [28]. Two types of theories are presented in the case of the plate formulation: (a) *complete* theories, (b) *different* theories. The *complete* models refer to the ones where the same expansion is adopted for all the displacement components. The use of *different* theories for each displacement variable is another interesting option; that is, each displacement component may be approximated using a distinct expansion. The second approach uses Lagrange polynomials. Thickness is approximated with Lagrange Points (LPs), and displacement is interpolated from these points [29]. Interpolation depends on the number of LPs. The points are defined in the natural coordinate $r = [-1, +1]$. Finally, a mixed ESL/LW approach can be advantageous for approximating the three-dimensional displacement field. In this method, displacement components are represented using either Lagrange or Taylor expansions, see also [21] for more details. In the present work, such formulations are termed TE/LE models.

Primal investigations into free-edge phenomena in composites include the early works of Hayashi [30], Puppo and Evensen [31], and Pipes and Pagano [32]. Several analytical approaches have yielded closed-form solutions for free-edge stress analysis [33–35]. Also, various numerical strategies have been employed. Early finite-element studies include the work of Wang and Crossman [36], who used three-node elements with mesh refinement near the free edge, and Whitcomb et al. [37], who analysed stress singularities with eight-node elements. Raju and Crews [38] adopted 3D solid elements, while Robbins and Reddy [39] employed a higher-order LW plate element. More recently, Vidal et al. [40] applied the proper generalized decomposition, discretizing the mid-plane with eight-node elements and using a refined fourth-order LW expansion through the thickness. Wang and Choi [41] studied the free-edge stress singularities by adopting a formulation based on Lekhknitskii's stress potentials. Davìand Milazzo [42] investigated normal and shear stresses by means of an analytical Boundary Element Method (BEM) solution. Mittelstedt and Becker [43] subsequently employed the Boundary Finite Element Method (BFEM) within the framework of linear elasticity for the analysis of three-dimensional stress states. More recently, Dölling et al. [44] proposed the use of the semi-analytical Scaled Boundary Finite Element Method (SBFEM). All these methods have demonstrated superior computational efficiency compared to classical FEM formulations. For further details, the reader is referred to the comprehensive review by Mittelstedt et al. [45] which covers recent developments in the study and characterization of the free-edge effect for various geometries and boundary conditions. Within the framework of the CUF, De Miguel et al. [46,47] employed advanced beam models to analyse free-edge stress fields and failure under various loading conditions. In addition, D'Ottavio et al. [48] investigated and compared higher-order and less-refined models in the context of the unified plate formulation. Stapleton et al. [49] later applied CUF to stress analysis in adhesively bonded double-lap joints. More recently, Scano et al. [50] investigated free-edge phenomena using a CUF-based two-dimensional sub-laminate method.

The enhanced accuracy of refined models is accompanied by significantly increased computational expense, especially in the analysis of local phenomena [51]. To mitigate this, hybrid modelling strategies have been developed. These approaches confine high-fidelity models to critical areas and use lower-fidelity models elsewhere. Despite their efficiency, implementing these global–local frameworks is complex. Consequently, numerous methodologies for coupling different structural theories have been proposed [52]. For instance, Fish et al. [53] introduced a multi-grid approach that exchanges information between coarse and fine meshes via an iterative algorithm. One of the most established techniques employs Lagrange multipliers, as discussed by Prager [54,55]. Alternative strategies include the use of spline methods to couple domains with non-matching meshes, as demonstrated by Aminpour et al. [56] and Ransom [57], and the three-field formulation presented by Brezzi and Marini [58]. More recently, Blanco et al. [59,60] developed the eXtended Variational Formulation (XVF), which couples distinct kinematic models using Lagrange multipliers. Compatibility between adjacent zones can also be ensured through an overlapping region. In this context, Ben Dhia and co-workers [61,62] proposed the Arlequin method, which enforces coupling constraints. This method was later implemented within the Carrera Unified Formulation (CUF) for plate models in purely mechanical analyses by Biscani et al. [63]. Subsequently, it was extended to the context of piezoelasticity in [64].

This paper presents enhanced 2D finite elements based on the Node-Dependent Kinematics (NDK) method [65–67], which allows each node to adopt different expansions and enables independent modelling of displacement variables without special coupling. Specifically, for a 2D problem, the expansion functions change across the plate mid-plane. The NDK approach has also been employed by Zappino and Carrera [68] for studying free-edge effects in thermoelastic problems. This method has also been assessed for the beam formulation [69]. The principal objective of the present work is to establish a finite element framework in which kinematic theories can be independently selected at each node, enabling a tailored balance between accuracy and computational efficiency, and ultimately leading to the generation of global/local models. By virtue of this capability, the proposed approach offers an efficient and flexible tool for the investigation of the free-edge phenomenon, which is inherently localized in nature and is therefore particularly well-suited to global/local analysis strategies. The first step involves developing a unified method that isolates the contributions of individual terms, eliminating the need to reformulate equations for each new theory. This method is the new advanced Unified Formulation, which has been previously cited in this Introduction, and more details will be given in Section 2. The second step leverages the possibility of adopting different structural theories for each node. This application of the NDK method provides the flexibility to combine low- and high-order theories within a single 2D model. The present contribution represents a natural continuation of previous works, constituting a further step towards the establishment of a general framework, as described at the end of the Introduction in [20]. In this context, Lagrange and Taylor polynomials are adopted to implement the LW and ESL approaches, respectively. In particular, Lagrange polynomials are chosen since they can effectively join different element types without requiring mathematical constructs such as Lagrange multipliers. This methodology extends previous work that successfully addressed analogous problems in beam structures [70].

Section 2 briefly revises the principles of the Unified Formulation and details the mathematics of the NDK method within the CUF plate framework. Section 3 derives the governing equations and presents the explicit form of the finite element matrices. Numerical results for shear and transverse stresses in the free-edge critical region are presented in Section 5. Finally, Section 6 summarizes the main findings and outlines potential future research directions.

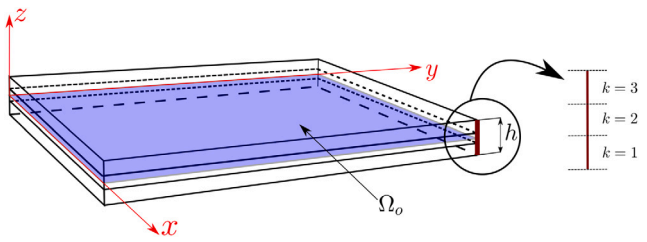


Fig. 1. Reference system for a generic multilayered two-dimensional plate.

2. Theoretical foundations

A multilayered plate is depicted in Fig. 1 within a reference system (x, y, z). The index k denotes the computational layer in the thickness direction (z-axis). The transverse fibre A is placed along the out-of-plane z-direction, with the mid-surface Ω_0 lying in the x–y plane. Thus, the three-dimensional displacement field can be expressed as follows:

$$\mathbf{u}^k(x^k, y^k, z^k) = \left\{ \begin{array}{ccc} u_x^k(x^k, y^k, z^k), & u_y^k(x^k, y^k, z^k), & u_z^k(x^k, y^k, z^k) \end{array} \right\}^T \quad (1)$$

2.1. Unified formulation for plates

The first step is to create a unified mathematical framework capable of representing all types of structural models for all three displacement variables, including both ESL and LW approaches. To this end, the Carrera Unified Formulation (CUF) permits a compact and versatile description of such models. The three-dimensional displacement field is thus reformulated as follows:

$$\begin{aligned} u_x^k &= F_{u_x\tau}^k(z^k) u_{x_\tau}^k(x^k, y^k) \quad \text{with} \quad \tau = 1, \dots, M_{u_x} \\ u_y^k &= F_{u_y\tau}^k(z^k) u_{y_\tau}^k(x^k, y^k) \quad \text{with} \quad \tau = 1, \dots, M_{u_y} \\ u_z^k &= F_{u_z\tau}^k(z^k) u_{z_\tau}^k(x^k, y^k) \quad \text{with} \quad \tau = 1, \dots, M_{u_z} \end{aligned} \quad (2)$$

where $F_{u_x\tau}^k$, $F_{u_y\tau}^k$, and $F_{u_z\tau}^k$ are the expansion functions for the displacements $u_{x_\tau}^k$, $u_{y_\tau}^k$, and $u_{z_\tau}^k$, respectively. The number of expansion terms for each displacement is given by M_{u_x}, M_{u_y}, and M_{u_z}.

As this work presents a numerical analysis, the finite element formulation is completed by discretizing the kinematic variables $u_{x_\tau}^k$, $u_{y_\tau}^k$, and $u_{z_\tau}^k$ using two-dimensional shape functions. Consequently, the displacement field is expressed as follows:

$$\begin{aligned} u_x^k &= N_i(x^k, y^k) F_{u_x\tau}^k(z^k) q_{x_{\tau i}}^k \quad \text{with} \quad \tau = 1, \dots, M_{u_x} \quad \text{and} \quad i = 1, \dots, N_n \\ u_y^k &= N_i(x^k, y^k) F_{u_y\tau}^k(z^k) q_{y_{\tau i}}^k \quad \text{with} \quad \tau = 1, \dots, M_{u_y} \quad \text{and} \quad i = 1, \dots, N_n \\ u_z^k &= N_i(x^k, y^k) F_{u_z\tau}^k(z^k) q_{z_{\tau i}}^k \quad \text{with} \quad \tau = 1, \dots, M_{u_z} \quad \text{and} \quad i = 1, \dots, N_n \end{aligned} \quad (3)$$

Here, N_i denotes the shape functions, where repeated subscript i implies summation, and N_n is the total number of shape functions per element. The unified formulation theoretically permits the use of every type of shape function. In the present paper, the focus is on the quadrilateral Lagrange-based finite elements. For the virtual system, the indices i and τ are replaced by j and s, respectively.

2.2. Node-dependent kinematics

In the previous Section, the through-thickness expansion functions remained consistent across the entire structural mid-plane. To enhance modelling flexibility, it may be advantageous to assign different kinematic theories to distinct regions of the plate. This objective is achieved through node-dependent kinematics, which allows each finite element node to be governed by its own independent structural theory.

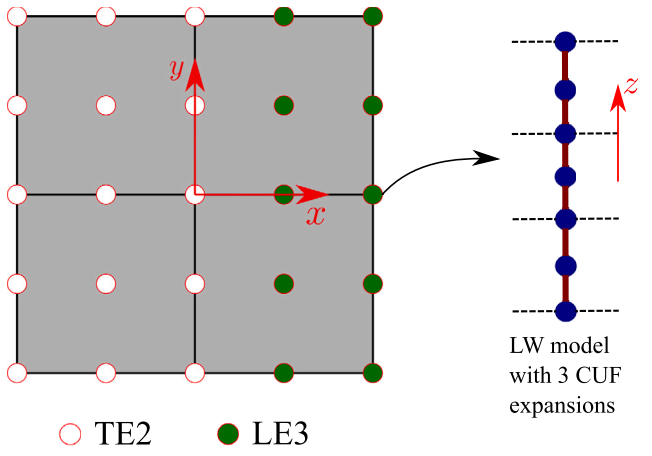


Fig. 2. The model employs four nine-node plate elements (Q9) featuring node-dependent kinematics, which combines a second-order Taylor expansion (TE2) and a parabolic LW Lagrange expansion (LE3) for each layer.

To better illustrate this concept, consider the finite element model presented in Fig. 2. The plate's mid-plane $(x - y)$ is discretized into four nine-node (Q9) elements. The nodes belonging to the two left-hand elements employ a full second-order Taylor expansion (TE2). The central nodes where TE2 is present are shared between adjacent elements; this guarantees a continuous kinematic transition across element boundaries without requiring Lagrange multipliers. For this reason, the two elements on the right utilize a mixed kinematic description, combining both the TE2 and a three-node Lagrange (LE3) expansion. The latter provides a parabolic, piecewise representation through the thickness.

Starting from Eq. (3), the NDK method can be formally expressed by introducing a nodal superscript i to the expansion functions F. The modified formulation reads:

$$\begin{aligned} u_x^k &= N_i(x, y) F_{u_x\tau}^{ki}(z) q_{x_{\tau i}}^k \quad \text{with} \quad \tau = 1, \dots, M_{u_x} \quad \text{and} \quad i = 1, \dots, N_n \\ u_y^k &= N_i(x, y) F_{u_y\tau}^{ki}(z) q_{y_{\tau i}}^k \quad \text{with} \quad \tau = 1, \dots, M_{u_y} \quad \text{and} \quad i = 1, \dots, N_n \\ u_z^k &= N_i(x, y) F_{u_z\tau}^{ki}(z) q_{z_{\tau i}}^k \quad \text{with} \quad \tau = 1, \dots, M_{u_z} \quad \text{and} \quad i = 1, \dots, N_n \end{aligned} \quad (4)$$

It is possible to adopt compact notations for real and virtual systems, as shown below:

$$u_l^k = N_i F_{u_l\tau}^{ki} q_{l_{\tau i}}^k = \sum_{i=1}^{N_n} \sum_{\tau=1}^{M_{u_l}} N_i F_{u_l\tau}^{ki} q_{l_{\tau i}}^k \quad (5)$$

$$\delta u_m^k = N_j F_{u_m s}^{kj} \delta q_{m_{sj}}^k = \sum_{j=1}^{N_n} \sum_{s=1}^{M_{u_m}} N_j F_{u_m s}^{kj} \delta q_{m_{sj}}^k \quad (6)$$

In this notation, $l, m \in \{x, y, z\}$ are coordinate indices. The summations over the nodal indices i (or j) and the kinematic term indices τ (or s) are expressed explicitly, whereas no summation is implied over the coordinate indices l and m. This form of the equations is particularly suited to the matrix assembly procedure for the linear system, developed in Section 3.

3. Governing equations and finite element matrices

The derivation of the governing equations begins with the definitions of the stress tensor, $\boldsymbol{\sigma}^k$, and the strain tensor, $\boldsymbol{\epsilon}^k$, from classical elasticity theory:

$$\begin{aligned} \boldsymbol{\sigma} &= \left\{ \begin{array}{cccccc} \sigma_{xx}^k & \sigma_{yy}^k & \sigma_{zz}^k & \sigma_{yz}^k & \sigma_{xz}^k & \sigma_{xy}^k \end{array} \right\}^T, \\ \boldsymbol{\epsilon}^k &= \left\{ \begin{array}{cccccc} \epsilon_{xx}^k & \epsilon_{yy}^k & \epsilon_{zz}^k & \epsilon_{yz}^k & \epsilon_{xz}^k & \epsilon_{xy}^k \end{array} \right\}^T \end{aligned} \quad (7)$$

The geometric relationships between strains and displacements are defined as follows:

$$\boldsymbol{\epsilon}^k = \mathbf{D}\mathbf{u}^k \tag{8}$$

where $\mathbf{D}$ represents the matrix of differential operators, applicable in the case of small displacements and angles of rotation:

$$\mathbf{D} = \begin{bmatrix} \partial_x & 0 & 0 \\ 0 & \partial_y & 0 \\ 0 & 0 & \partial_z \\ 0 & \partial_z & \partial_y \\ \partial_z & 0 & \partial_x \\ \partial_y & \partial_x & 0 \end{bmatrix} \tag{9}$$

The analysis considers linear elastic, orthotropic materials, which are governed by the constitutive relation:

$$\boldsymbol{\sigma}^k = \mathbf{C}^k \boldsymbol{\epsilon}^k \tag{10}$$

where $\mathbf{C}^k$ is the matrix of the material coefficients:

$$\mathbf{C}^k = \begin{bmatrix} C_{11}^k & C_{12}^k & C_{13}^k & 0 & 0 & C_{16}^k \\ C_{21}^k & C_{22}^k & C_{23}^k & 0 & 0 & C_{26}^k \\ C_{31}^k & C_{32}^k & C_{33}^k & 0 & 0 & C_{36}^k \\ 0 & 0 & 0 & C_{44}^k & C_{45}^k & 0 \\ 0 & 0 & 0 & C_{45}^k & C_{55}^k & 0 \\ C_{61}^k & C_{62}^k & C_{63}^k & 0 & 0 & C_{66}^k \end{bmatrix} \tag{11}$$

It is noted that the previous equation holds in a reference frame rotated about the z-axis.

3.1. Derivation of the governing equations

The governing equations for the novel plate elements are derived by applying the principle of virtual work (see also the influential book of Washizu [71]), which states:

$$\delta L_{int} = \delta L_{ext} \tag{12}$$

Using the explicit expressions of the internal and external works, it is possible to write down:

$$\begin{aligned} &\int_V \delta\boldsymbol{\epsilon}^{kT}\boldsymbol{\sigma}^k \mathrm{d}V = \delta\mathbf{u}^{kT}\mathbf{P}^k = \\ &\int_V \left(\delta\epsilon_{xx}^k\sigma_{xx}^k + \delta\epsilon_{yy}^k\sigma_{yy}^k + \delta\epsilon_{zz}^k\sigma_{zz}^k + \delta\epsilon_{yz}^k\sigma_{yz}^k + \delta\epsilon_{xz}^k\sigma_{xz}^k + \delta\epsilon_{xy}^k\sigma_{xy}^k\right)\mathrm{d}V^k = \\ &\delta q_{x_{sj}}^k N_j F_{u_x s}^{kj} P_{u_x}^k + \delta q_{y_{sj}}^k N_j F_{u_y s}^{kj} P_{u_y}^k + \delta q_{z_{sj}}^k N_j F_{u_z s}^{kj} P_{u_z}^k \end{aligned} \tag{13}$$

where $\mathrm{d}V^k = \mathrm{d}x^k\mathrm{d}y^k\mathrm{d}z^k$. Moreover, the external work is computed for the point loads. The governing equations for each of the three virtual displacements are derived by combining the displacement-strain relation (Eq. (8)), the CUF and FEM approximations (Eqs. (5) and (6)), and the constitutive equations (Eq. (10)):

$$\begin{aligned} \delta q_{x_{sj}}^k &: K_{u_x u_x s\tau ji}^k q_{x_{\tau i}}^k + K_{u_x u_y s\tau ji}^k q_{y_{\tau i}}^k + K_{u_x u_z s\tau ji}^k q_{z_{\tau i}}^k = P_{u_x sj}^k \\ \delta q_{y_{sj}}^k &: K_{u_y u_x s\tau ji}^k q_{x_{\tau i}}^k + K_{u_y u_y s\tau ji}^k q_{y_{\tau i}}^k + K_{u_y u_z s\tau ji}^k q_{z_{\tau i}}^k = P_{u_y sj}^k \\ \delta q_{z_{sj}}^k &: K_{u_z u_x s\tau ji}^k q_{x_{\tau i}}^k + K_{u_z u_y s\tau ji}^k q_{y_{\tau i}}^k + K_{u_z u_z s\tau ji}^k q_{z_{\tau i}}^k = P_{u_z sj}^k \end{aligned} \tag{14}$$

3.2. Explicit expressions of the fundamental nuclei

It can be observed that among the previous equations, nine Fundamental Nuclei of the stiffness matrix share a similar mathematical structure. For the sake of completeness, their explicit expression are given below:

$$\begin{aligned} K_{u_x u_x s\tau ji}^k = {} & C_{11}^k \int_\Omega N_{j,x} N_{i,x} \mathrm{d}x^k\mathrm{d}y^k \int_{A_k} F_{u_x s}^{jk} F_{u_x \tau}^{ik} \mathrm{d}z^k \\ & + C_{55}^k \int_\Omega N_j N_i \mathrm{d}x^k\mathrm{d}y^k \int_{A_k} F_{u_x s,z}^{jk} F_{u_x \tau,z}^{ik} \mathrm{d}z^k \\ & + C_{66}^k \int_\Omega N_{j,y} N_{i,y} \mathrm{d}x^k\mathrm{d}y^k \int_{A_k} F_{u_x s}^{jk} F_{u_x \tau}^{ik} \mathrm{d}z^k \\ & + C_{16}^k \int_\Omega N_{j,y} N_{i,x} \mathrm{d}x^k\mathrm{d}y^k \int_{A_k} F_{u_x s}^{jk} F_{u_x \tau}^{ik} \mathrm{d}z^k \\ & + C_{16}^k \int_\Omega N_{j,x} N_{i,y} \mathrm{d}x^k\mathrm{d}y^k \int_{A_k} F_{u_x s}^{jk} F_{u_x \tau}^{ik} \mathrm{d}z^k \end{aligned} \tag{15}$$

$$\begin{aligned} K_{u_x u_y s\tau ji}^k = {} & C_{45}^k \int_\Omega N_j N_i \mathrm{d}x^k\mathrm{d}y^k \int_{A_k} F_{u_x s,z}^{jk} F_{u_y \tau,z}^{ik} \mathrm{d}z^k \\ & + C_{26}^k \int_\Omega N_{j,y} N_{i,y} \mathrm{d}x^k\mathrm{d}y^k \int_{A_k} F_{u_x s}^{jk} F_{u_y \tau}^{ik} \mathrm{d}z^k \\ & + C_{12}^k \int_\Omega N_{j,y} N_{i,x} \mathrm{d}x^k\mathrm{d}y^k \int_{A_k} F_{u_x s}^{jk} F_{u_y \tau}^{ik} \mathrm{d}z^k \\ & + C_{66}^k \int_\Omega N_{j,x} N_{i,y} \mathrm{d}x^k\mathrm{d}y^k \int_{A_k} F_{u_x s}^{jk} F_{u_y \tau}^{ik} \mathrm{d}z^k \\ & + C_{26}^k \int_\Omega N_{j,x} N_{i,x} \mathrm{d}x^k\mathrm{d}y^k \int_{A_k} F_{u_x s}^{jk} F_{u_y \tau}^{ik} \mathrm{d}z^k \end{aligned} \tag{16}$$

$$\begin{aligned} K_{u_x u_z s\tau ji}^k = {} & C_{13}^k \int_\Omega N_{i,x} N_j \mathrm{d}x^k\mathrm{d}y^k \int_{A_k} F_{u_x s,z}^{jk} F_{u_z \tau}^{ik} \mathrm{d}z^k \\ & + C_{55}^k \int_\Omega N_{j,x} N_i \mathrm{d}x^k\mathrm{d}y^k \int_{A_k} F_{u_x s}^{jk} F_{u_z \tau,z}^{ik} \mathrm{d}z^k \\ & + C_{45}^k \int_\Omega N_{j,y} N_i \mathrm{d}x^k\mathrm{d}y^k \int_{A_k} F_{u_x s}^{jk} F_{u_z \tau,z}^{ik} \mathrm{d}z^k \\ & + C_{36}^k \int_\Omega N_{i,y} N_j \mathrm{d}x^k\mathrm{d}y^k \int_{A_k} F_{u_x s,z}^{jk} F_{u_z \tau}^{ik} \mathrm{d}z^k \end{aligned} \tag{17}$$

$$\begin{aligned} K_{u_y u_x s\tau ji}^k = {} & C_{12}^k \int_\Omega N_{j,x} N_{i,y} \mathrm{d}x^k\mathrm{d}y^k \int_{A_k} F_{u_y s}^{jk} F_{u_x \tau}^{ik} \mathrm{d}z^k \\ & + C_{66}^k \int_\Omega N_{j,y} N_{i,x} \mathrm{d}x^k\mathrm{d}y^k \int_{A_k} F_{u_y s}^{jk} F_{u_x \tau}^{ik} \mathrm{d}z^k \\ & + C_{45}^k \int_\Omega N_j N_i \mathrm{d}x^k\mathrm{d}y^k \int_{A_k} F_{u_y s,z}^{jk} F_{u_x \tau,z}^{ik} \mathrm{d}z^k \\ & + C_{26}^k \int_\Omega N_{j,y} N_{i,y} \mathrm{d}x^k\mathrm{d}y^k \int_{A_k} F_{u_y s}^{jk} F_{u_x \tau}^{ik} \mathrm{d}z^k \\ & + C_{16}^k \int_\Omega N_{j,x} N_{i,x} \mathrm{d}x^k\mathrm{d}y^k \int_{A_k} F_{u_y s}^{jk} F_{u_x \tau}^{ik} \mathrm{d}z^k \end{aligned} \tag{18}$$

$$\begin{aligned} K_{u_y u_y s\tau ji}^k = {} & C_{22}^k \int_\Omega N_{j,y} N_{i,y} \mathrm{d}x^k\mathrm{d}y^k \int_{A_k} F_{u_y s}^{jk} F_{u_y \tau}^{ik} \mathrm{d}z^k \\ & + C_{44}^k \int_\Omega N_j N_i F_{u_y s,z}^{jk} F_{u_y \tau,z}^{ik} \mathrm{d}z^k \\ & + C_{66}^k \int_\Omega N_{j,x} N_{i,x} \mathrm{d}x^k\mathrm{d}y^k \int_{A_k} F_{u_y s}^{jk} F_{u_y \tau}^{ik} \mathrm{d}z^k \\ & + C_{26}^k \int_\Omega N_{j,y} N_{i,x} \mathrm{d}x^k\mathrm{d}y^k \int_{A_k} F_{u_y s}^{jk} F_{u_y \tau}^{ik} \mathrm{d}z^k \\ & + C_{26}^k \int_\Omega N_{j,x} N_{i,y} \mathrm{d}x^k\mathrm{d}y^k \int_{A_k} F_{u_y s}^{jk} F_{u_y \tau}^{ik} \mathrm{d}z^k \end{aligned} \tag{19}$$

$$\begin{aligned} K_{u_y u_z s\tau ji}^k = {} & C_{45}^k \int_\Omega N_{j,x} N_i \mathrm{d}x^k\mathrm{d}y^k \int_{A_k} F_{u_y s}^{jk} F_{u_z \tau,z}^{ik} \mathrm{d}z^k \\ & + C_{36}^k \int_\Omega N_{i,x} N_j \mathrm{d}x^k\mathrm{d}y^k \int_{A_k} F_{u_y s,z}^{jk} F_{u_z \tau}^{ik} \mathrm{d}z^k \\ & + C_{23}^k \int_\Omega N_{i,y} N_j \mathrm{d}x^k\mathrm{d}y^k \int_{A_k} F_{u_y s,z}^{jk} F_{u_z \tau}^{ik} \mathrm{d}z^k \\ & + C_{44}^k \int_\Omega N_{j,y} N_i \mathrm{d}x^k\mathrm{d}y^k \int_{A_k} F_{u_y s}^{jk} F_{u_z \tau,z}^{ik} \mathrm{d}z^k \end{aligned} \tag{20}$$

$$\begin{aligned} K_{u_z u_x s\tau ji}^k = {} & C_{13}^k \int_\Omega N_{j,x} N_i \mathrm{d}x^k\mathrm{d}y^k \int_{A_k} F_{u_z s}^{jk} F_{u_x \tau,z}^{ik} \mathrm{d}z^k \\ & + C_{55}^k \int_\Omega N_j N_{i,x} \mathrm{d}x^k\mathrm{d}y^k \int_{A_k} F_{u_z s,z}^{jk} F_{u_x \tau}^{ik} \mathrm{d}z^k \end{aligned}$$

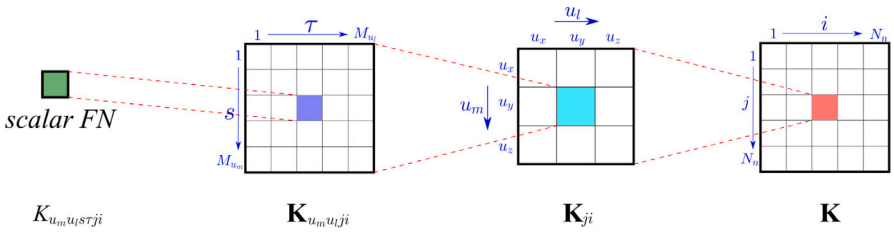


Fig. 3. General procedure of the assembly for the stiffness matrix.

$$
\begin{aligned}
&+ C^k_{36} \int_\Omega N_{j,y} N_i \mathrm{d}x^k \mathrm{d}y^k \int_{A_k} F^{jk}_{u_z s} F^{ik}_{u_x \tau,z} \mathrm{d}z^k \\
&+ C^k_{45} \int_\Omega N_j N_{i,y} \mathrm{d}x^k \mathrm{d}y^k \int_{A_k} F^{jk}_{u_z s,z} F^{ik}_{u_x \tau} \mathrm{d}z^k
\end{aligned} \tag{21}
$$

$$
\begin{aligned}
K^k_{u_z u_y s \tau j i} &= C^k_{23} \int_\Omega N_{j,y} N_i \mathrm{d}x^k \mathrm{d}y^k \int_{A_k} F^{jk}_{u_z s} F^{ik}_{u_y \tau,z} \mathrm{d}z^k \\
&+ C^k_{44} \int_\Omega N_j N_{i,y} \mathrm{d}x^k \mathrm{d}y^k \int_{A_k} F^{jk}_{u_z s,z} F^{ik}_{u_y \tau} \mathrm{d}z^k \\
&+ C^k_{36} \int_\Omega N_{j,x} N_i \mathrm{d}x^k \mathrm{d}y^k \int_{A_k} F^{jk}_{u_z s} F^{ik}_{u_y \tau,z} \mathrm{d}z^k \\
&+ C^k_{45} \int_\Omega N_j N_{i,x} \mathrm{d}x^k \mathrm{d}y^k \int_{A_k} F^{jk}_{u_z s,z} F^{ik}_{u_y \tau} \mathrm{d}z^k
\end{aligned} \tag{22}
$$

$$
\begin{aligned}
K^k_{u_z u_z s \tau j i} &= C^k_{33} \int_\Omega N_j N_i \mathrm{d}x^k \mathrm{d}y^k \int_{A_k} F^{jk}_{u_z s,z} F^{ik}_{u_z \tau,z} \mathrm{d}z^k \\
&+ C^k_{44} \int_\Omega N_{j,y} N_{i,y} \mathrm{d}x^k \mathrm{d}y^k \int_{A_k} F^{jk}_{u_z s} F^{ik}_{u_z \tau} \mathrm{d}z^k \\
&+ C^k_{55} \int_\Omega N_{j,x} N_{i,x} \mathrm{d}x^k \mathrm{d}y^k \int_{A_k} F^{jk}_{u_z s} F^{ik}_{u_z \tau} \mathrm{d}z^k \\
&+ C^k_{45} \int_\Omega N_{j,y} N_{i,x} \mathrm{d}x^k \mathrm{d}y^k \int_{A_k} F^{jk}_{u_z s} F^{ik}_{u_z \tau} \mathrm{d}z^k \\
&+ C^k_{45} \int_\Omega N_{j,x} N_{i,y} \mathrm{d}x^k \mathrm{d}y^k \int_{A_k} F^{jk}_{u_z s} F^{ik}_{u_z \tau} \mathrm{d}z^k
\end{aligned} \tag{23}
$$

It is worth remarking that the volume integral has been decomposed into two distinct contributions: the first is associated with the FEM discretization, whereas the second depends exclusively on the expansion functions along the thickness direction. Also, the material coefficients are placed outside the integrals, as they do not depend on (x, y, z).

Similarly, the three fundamental scalar nuclei of the load vector are:

$$
\begin{aligned}
P^k_{u_x sj} &= N_j F^{kj}_{u_x s} P^k_{u_x} \\
P^k_{u_y sj} &= N_j F^{kj}_{u_y s} P^k_{u_y} \\
P^k_{u_z sj} &= N_j F^{kj}_{u_z s} P^k_{u_z}
\end{aligned} \tag{24}
$$

4. Assembly

This research proposes a novel formulation of the Fundamental Nucleus (FN), which represents a shift from the classical CUF methodology. The first modification is the scalar representation of the FN components. In particular, the stiffness terms $K^k_{u_m u_l s \tau j i}$ and the load terms $P^k_{u_m sj}$ are treated as independent scalar components rather than being embedded within a conventional 3×3 matrix (or 3×1 in the case of the load vector). As shown in the preceding section, this approach requires only nine independent scalar parameters for the stiffness matrix and three for the load array. Furthermore, it provides significant theoretical improvements over the standard CUF framework [3,15], most importantly by removing the constraint that enforces a uniform expansion theory and numerical approach across all displacement variables, a constraint that typically leads to redundant computations in traditional implementations.

Fig. 3 illustrates the general procedure for the assemblage of the stiffness matrix. The procedure originates from the invariant kernel $K^k_{u_m u_l s \tau j i}$, which is expanded through successive operations. First, expansion with respect to the indices s and τ yields the submatrix $\mathbf{K}_{u_m u_l j i}$. This submatrix is then expanded over the displacement components u_m and u_l, arriving at $\mathbf{K}_{ji}$. Finally, the expansion with respect to the nodal indices j and i produces the complete structural stiffness matrix $\mathbf{K}$. Carrera and Scano [70] proposed an analogous assemblage procedure for beam elements.

Example for a single element. In this paragraph, a simple example is illustrated to help the understanding of the FE matrix assembly process within the plate Unified Formulation using the NDK method. To this end, Fig. 4 depicts a four-node quadrilateral element (Q4); however, the same assembly concept applies to the nine-node quadrilateral (Q9) elements employed in the present analyses, or to other types of shape functions. In the first node, the FSDT is adopted, that is, two terms are used for u_x and u_y, and only a constant term is used for u_z. For the other three FE nodes, a third-order Taylor model, TE3, is adopted for each displacement component. In practice, the first node has 5 terms, while the other nodes have 12 terms. The total number of degrees of freedom for the entire structure is 41.

The assembled global stiffness matrix $\mathbf{K}$ is presented in Fig. 5 and has dimensions 41×41. Due to node-dependent kinematics, the number of degrees of freedom varies from node to node. Consequently, the submatrices $\mathbf{K}_{ji}$ can have different dimensions, as visually detailed in the figure. The assembly process is further detailed in Fig. 6, which shows how a submatrix $\mathbf{K}_{ji}$ is partitioned into nine distinct sub-arrays. Each sub-array consists of a set of scalar FN, where the count of nuclei is governed by the number of expansion terms for the corresponding FE node and displacement component. This results in sub-blocks $\mathbf{K}_{u_m u_l j i}$ with differing dimensions and shapes. For clarity, the figure displays four representative examples that highlight the dimensional diversity.

5. Numerical results

This section proposes a detailed analysis of out-of-plane stress fields in the free-edge region of two examples. The first example assesses a benchmark case from the open literature for two different laminate stacking sequences. On the other hand, the second example analyses a 32-layer structure, comparing results from the present formulation with those obtained from refined three-dimensional solid models in ABAQUS. This case could be used as a new benchmark for future research.

In the present examples, the analysis employs four modelling approaches: (a) uniform Taylor expansion models, (b) uniform Lagrange expansion models, (c) mixed TE/LE models, and (d) NDK models. For cases (a) through (c), a single kinematic theory is applied uniformly across all nodes. For case (d), the distribution of different kinematic theories over the mid-plane of the plates will be illustrated graphically; such configurations will be referred to as NDKn. The NDK formulation divides the domain into Global and Local kinematic zones. While the methodology allows for an arbitrary number of zones, the current study is restricted to only two. Additional implementation details are explained for each benchmark. The classical nine-node Lagrange element (Q9) is employed for all the analyses [72]. It should be noted

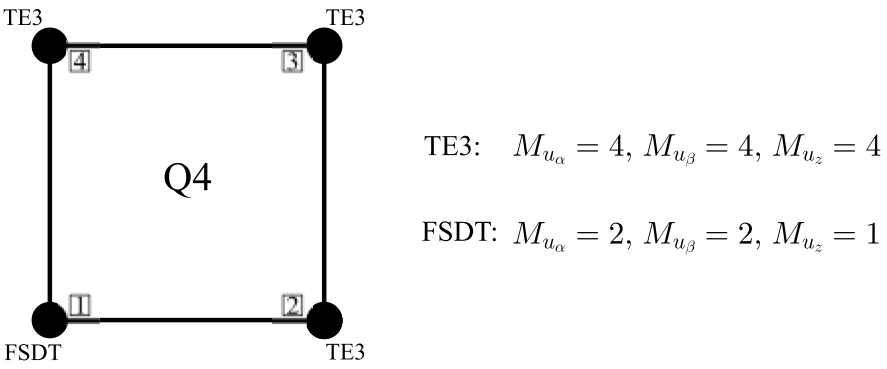


Fig. 4. Example of a plate element. The first node adopts the FSDT classical expansion, while the others use the complete third-order Taylor expansion (TE3).

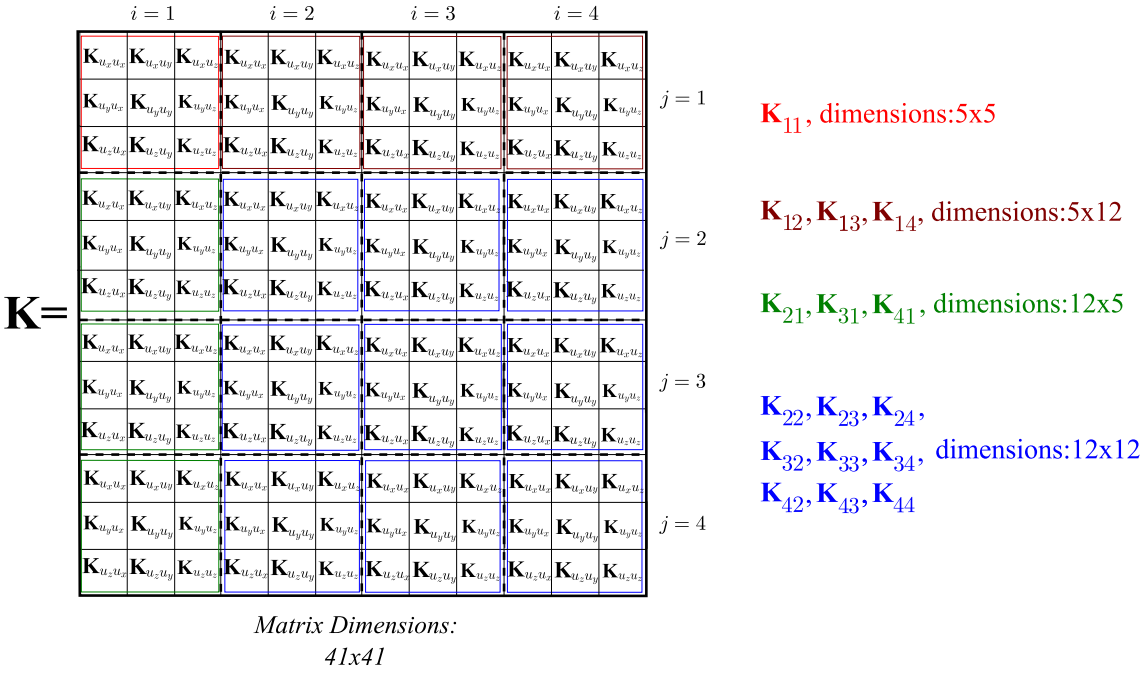


Fig. 5. Assemblage of the structural stiffness matrix.

that both shear and transverse normal stresses are calculated using the constitutive law. In particular, no stress recovery method has been adopted.

5.1. Assessment from the literature

The first benchmark examines the free-edge behaviour of a composite plate with a rectangular surface of length $L = 40$ [mm], width $b = 20$ [mm], and thickness $h = 5$ [mm], as illustrated in Fig. 7. Two symmetric laminates are considered:

- A four-layer $[45°/-45°]_s$ laminate, see Fig. 7(a).
- An eight-layer quasi-isotropic $[90°/0°/45°/-45°]_s$ laminate, see Fig. 7(b).

For both laminates, the material properties are: $E_1 = 137.9$ [GPa], $E_2 = E_3 = 14.5$ [GPa], $\nu_{12} = \nu_{13} = \nu_{23} = 0.21$, and $G_{12} = G_{13} = G_{23} = 5.9$ [GPa]. As in the reference Scano et al. [50], the plate is subjected to a uniform axial strain ϵ_0 along the x-axis by imposing a prescribed displacement $\bar{u}$ at $x = \pm L/2$. This loading produces a constant strain field in the central region of the plate, provided the length L is sufficiently large relative to the edge-affected zones. Given the need for higher resolution near the free edge, both laminates are modelled using a non-uniform 16×16 finite element mesh, as shown in Fig. 8. The FE mesh on the mid-plane is divided into two zones. (a) The refined local region contains 208 FE nodes, where more detailed kinematic theories are applied. (b) The larger global region has 881 FE nodes, where computationally efficient theories are used.

The analysis focuses on the out-of-plane stress components: the shear stress σ_{xz} and the transverse normal stress σ_{zz}. These are computed along the thickness direction at a point close to the free edge ($y/b = 0.998$) and at the mid-plane in the x-direction ($x = 0$). As it is common in the literature, the results are presented in the following scaled form:

$$\overline{\sigma}_{xz} = \frac{\sigma_{xz}}{\epsilon_0} \qquad \overline{\sigma}_{zz} = \frac{\sigma_{zz}}{\epsilon_0} \tag{25}$$

Four-layer case. First, the four-layer laminate $[45°/-45°]_s$ is considered. When the LW approach is used, one LE7 (sixth order) expansion is assigned to each material layer, resulting in four CUF elements through the thickness, consistent with the reference result in [50]. Table 1 provides an overview of the Unified Formulation models, specifying for each case the Global Model, the Local Model, the total number of Degrees of Freedom (DOF), and the resulting DOF reduction. This reduction is defined according to the following expression:

$$\text{DOF Reduction} = \left\| \frac{\text{DOF (LE7)} - \text{DOF (Theory)}}{\text{DOF (LE7)}} \right\| \times 100 \tag{26}$$

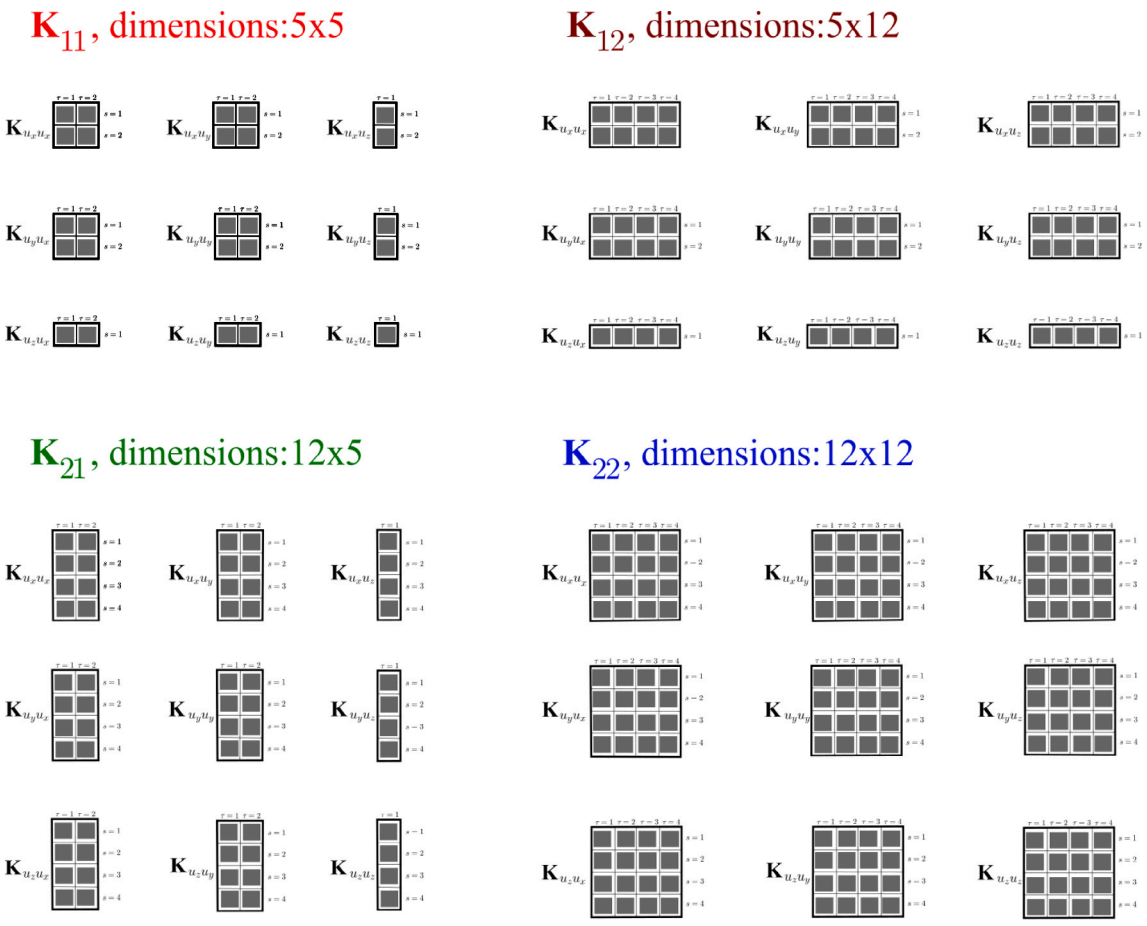


Fig. 6. Detailed illustration for a part of the stiffness matrix.

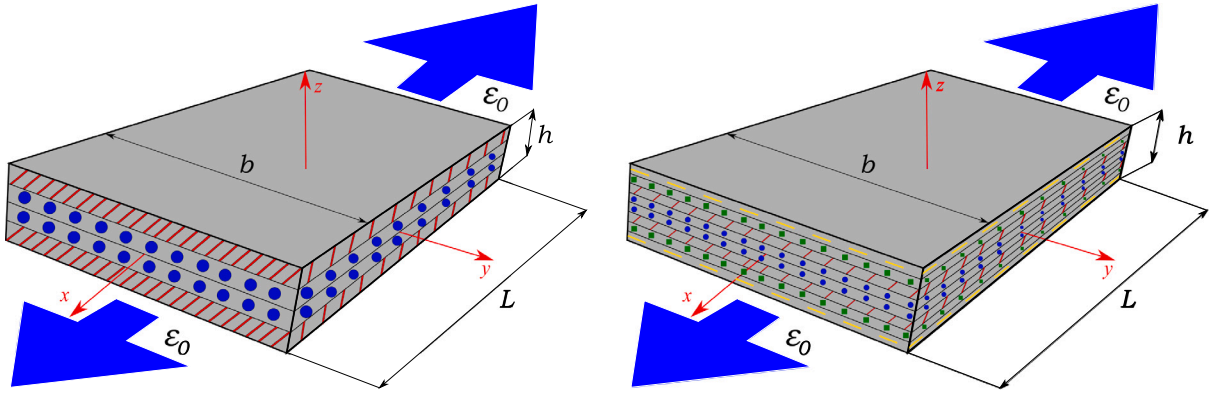


Fig. 7. Geometrical properties for the composite plate.
Source: The study case is taken from [39,50].

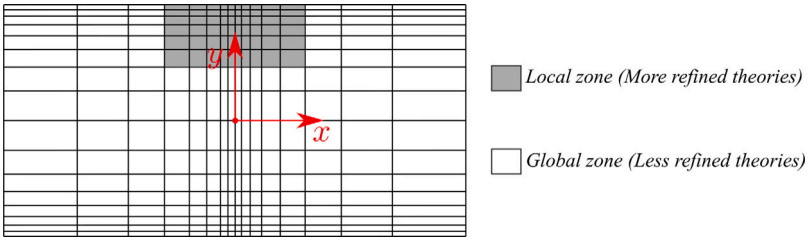


Fig. 8. NDK mesh. The nodes with refined theories are collocated around the studied zone.

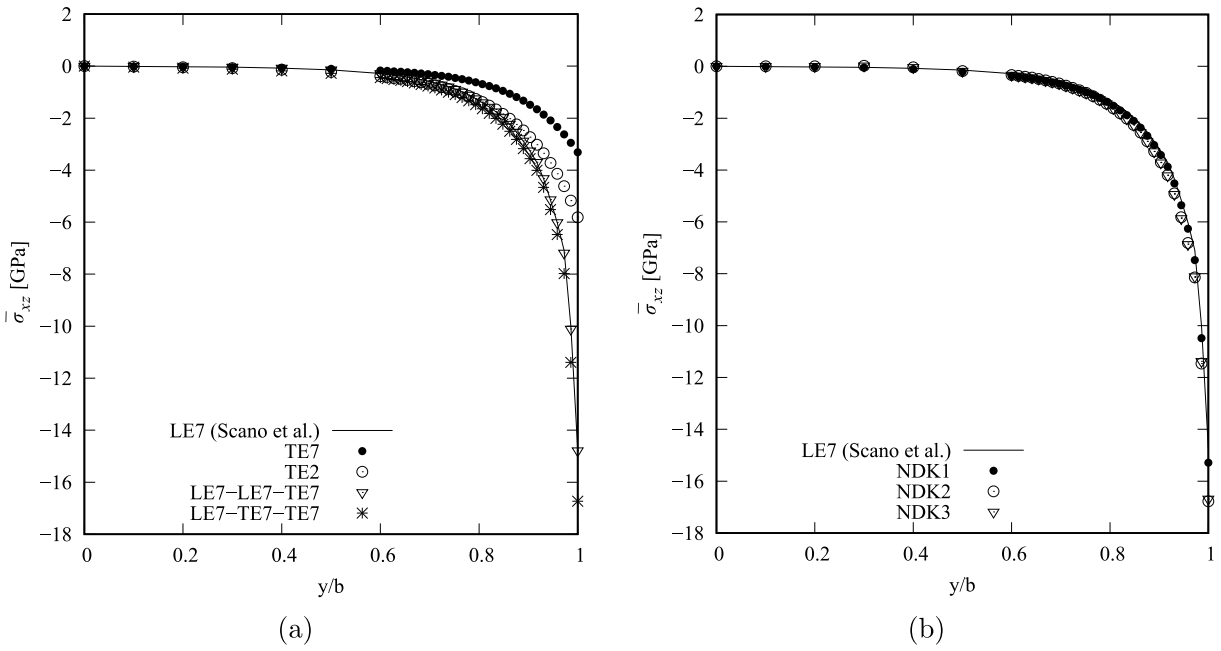


Fig. 9. Shear stresses, σ_{xz}, along y of the angle-ply $[45°/-45°]_s$ laminate at the interface $45°/(-45°)$.

Table 1
Unified formulation models used for the angle-ply $[45°/-45°]_s$ laminate.

Global model	Local model	DOF	DOF reduction [%]	Theory definition
Uniform models				
LE7-LE7-LE7	LE7-LE7-LE7	81 675	–[a]	LE7 (Scano et al.)
TE7-TE7-TE7	TE7-TE7-TE7	26 136	68.00	TE7
TE2-TE2-TE2	TE2-TE2-TE2	9801	88.00	TE2
TE-LE models				
LE7-LE7-TE7	LE7-LE7-TE7	63 162	22.67	LE7-LE7-TE7
LE7-TE7-TE7	LE7-TE7-TE7	44 649	45.33	LE7-TE7-TE7
NDK models				
TE2-TE2-TE2	LE7-LE7-TE7	19 993	75.52	NDK1
TE1-TE1-TE1	LE7-LE7-TE7	17 350	78.66	NDK2
TE1-TE1-TE1	LE7-LE7-LE7	20 866	74.45	NDK3

[a] Taken as the reference solution.

The last column of Table 1 provides the naming conventions used in subsequent figures. Together with Fig. 8, this table fully defines all theories employed. The table is organized into three sections: the top rows list three uniform models, the middle rows describe mixed TE-LE models, and the bottom rows present three NDK models. The selection of Taylor polynomials for the in-plane displacement component u_y is intentional, as it demonstrates that the evaluation of σ_{xz} depends only weakly on u_y, while the accurate computation of σ_{zz} is significantly affected by this component.

Fig. 9 depicts the variation of the shear components along the positive y- axis at the layer between the 45° and (−45°) layers. Fig. 10 shows the distribution of the shear stress, σ_{xz}, and Fig. 11 shows the corresponding transverse stress, σ_{zz}. The stresses are compared with the trends from Robbins and Reddy [39]. In both figures, the left-hand side presents results for uniform and mixed TE-LE models, while the right-hand side displays results for the NDK models.

Based on the analyses presented above, the following conclusions can be drawn:

- Uniform Taylor expansion models fail to match the reference solution, highlighting their inadequacy for capturing local free-edge effects.
- Accurate prediction of out-of-plane stresses requires higher-order LW kinematics, even when the in-plane displacement components (u_x, u_y) are well captured.
- All TE-LE and NDK models accurately compute the shear stress, σ_{xz}, whereas an accurate transverse stress, σ_{zz}, demands higher-fidelity approximations. In particular, they are able to calculate to identify the presence of relevant peaks at the interface between layers 45° and −45°.
- The results confirm that the traction-free condition is not satisfied for Taylor expansions. While the condition is always met for the shear stresses when LE is used for u_x, only NDK3 is able to satisfy it for the transverse normal stress. Also, the proposed global/local models follow the same stress gradients along the y-axis as in the complete reference solution.
- A significant computational advantage is achieved by combining a lower-order model over most of the domain with a refined local model confined to a small region of the two-dimensional mesh.
- The three proposed NDK models are highly efficient, showing excellent agreement with the reference results while achieving a DOF reduction exceeding 73%, outperforming even the TE7 model. In particular, the results demonstrate that a linear kinematic model (TE1) can be effectively used for the transverse displacement, u_z, even within the global zone.
- Among the presented models, only NDK3 accurately matches the reference results for both the shear and transverse normal stresses.

Eight-layer case. Then, the eight-layer quasi-isotropic laminate $[90°/0°/0°/45°/-45°]_s$ is taken into account. Differently from the previous case, one LE4 expansion can be assigned per material layer, yielding eight CUF elements through the thickness. This choice aligns with the reference results from [50]. The characteristics of the Unified Formulation models for the quasi-isotropic laminate are listed in Table 2. It follows the same format as Table 1, and the degree-of-freedom (DOF) reduction is again defined as:

$$\text{DOF Reduction} = \left\| \frac{\text{DOF (LE4)} - \text{DOF (Theory)}}{\text{DOF (LE4)}} \right\| \times 100 \tag{27}$$

The shear stress distributions are shown in Fig. 12, and the transverse stresses are shown in Fig. 13. The results were further validated

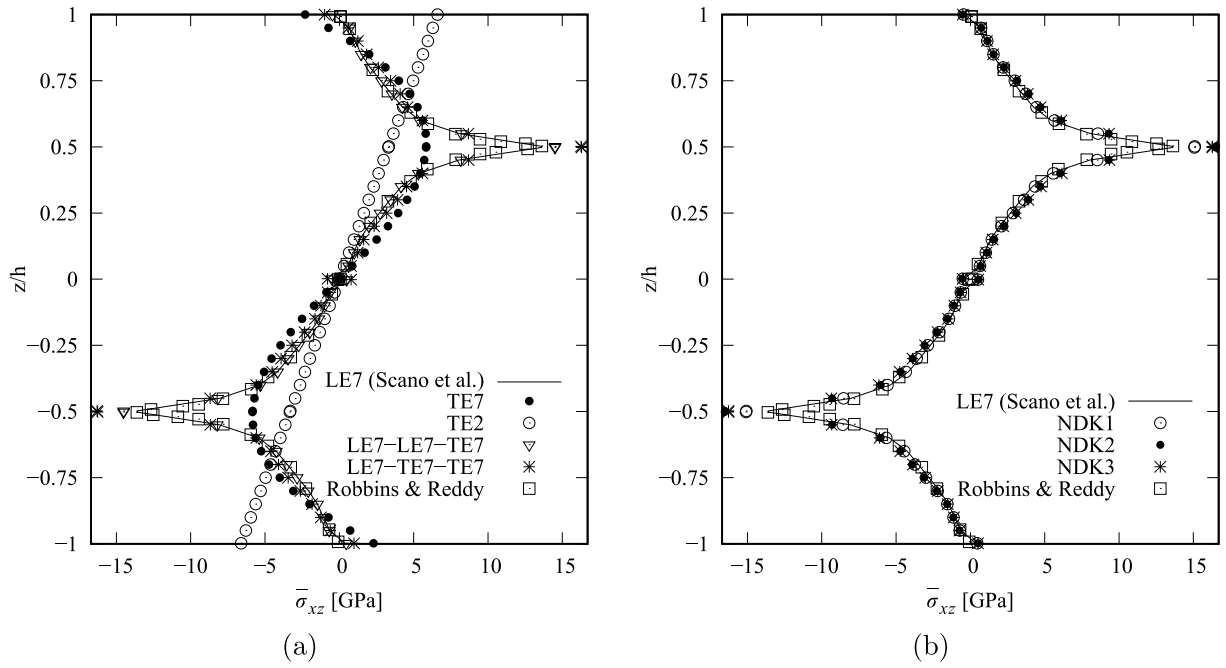


Fig. 10. Shear stresses, σ_{xz}, along z of the angle-ply $[45°/-45°]_s$ laminate.

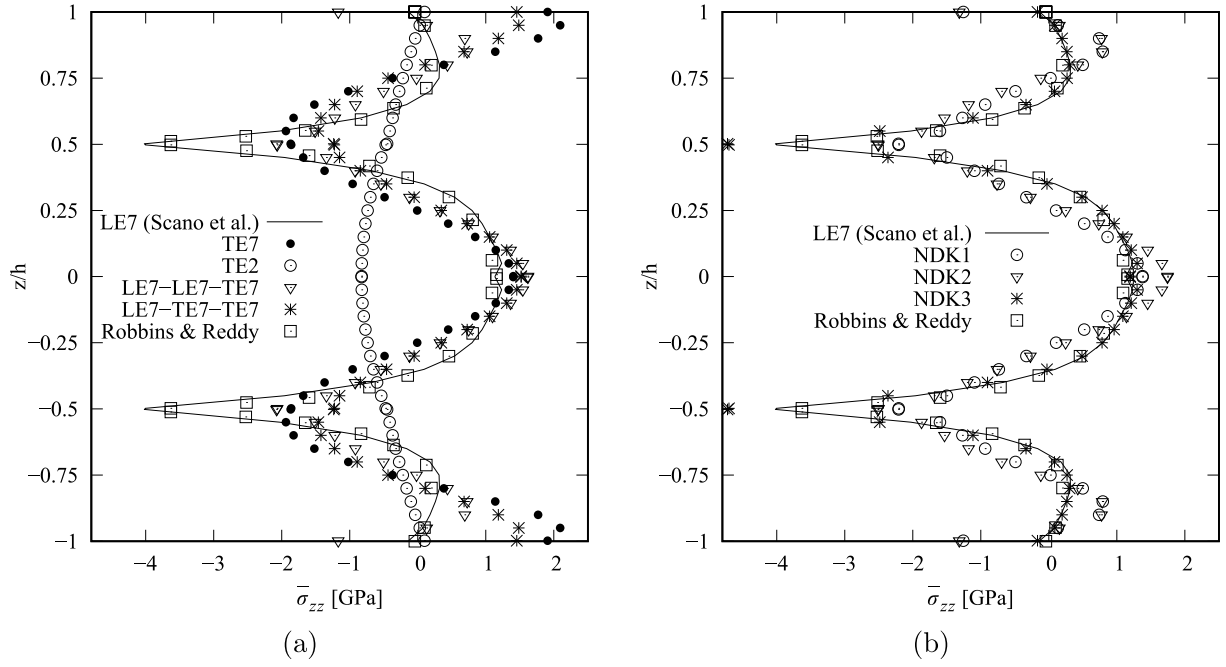


Fig. 11. Transverse stresses, σ_{zz}, along z of the angle-ply $[45°/-45°]_s$ laminate.

against the reference solution of Gaudenzi et al. [73]. In both figures, results obtained with uniform and mixed TE-LE models are displayed on the left, while those from NDK models appear on the right.

Based on the analysis of the quasi-isotropic laminate, the following conclusions can be drawn:

- Consistent with the four-layer case, uniform Taylor expansion models produce poor accuracy and are inadequate for capturing the free-edge stress field.
- Accurate out-of-plane stress prediction requires higher-order layer-wise kinematics, even when the in-plane displacements (u_x, u_y) are well represented.
- All TE-LE and NDK models capture the shear stress accurately, whereas the transverse stress requires higher-fidelity models. Notably, results from LE4-TE7-TE7 configurations indicate that a layer-wise description of u_x alone may suffice for accurate shear stress analysis. The results show that peaks arise at 90°-0° interface. The same considerations regarding the traction-free conditions as in the previous benchmarks apply here.
- The four proposed NDK models are computationally efficient, showing excellent agreement with the reference solution while reducing degrees of freedom (DOF) by more than 73%. Among them, NDK3 is particularly effective, achieving 82% DOF reduction without compromising accuracy.

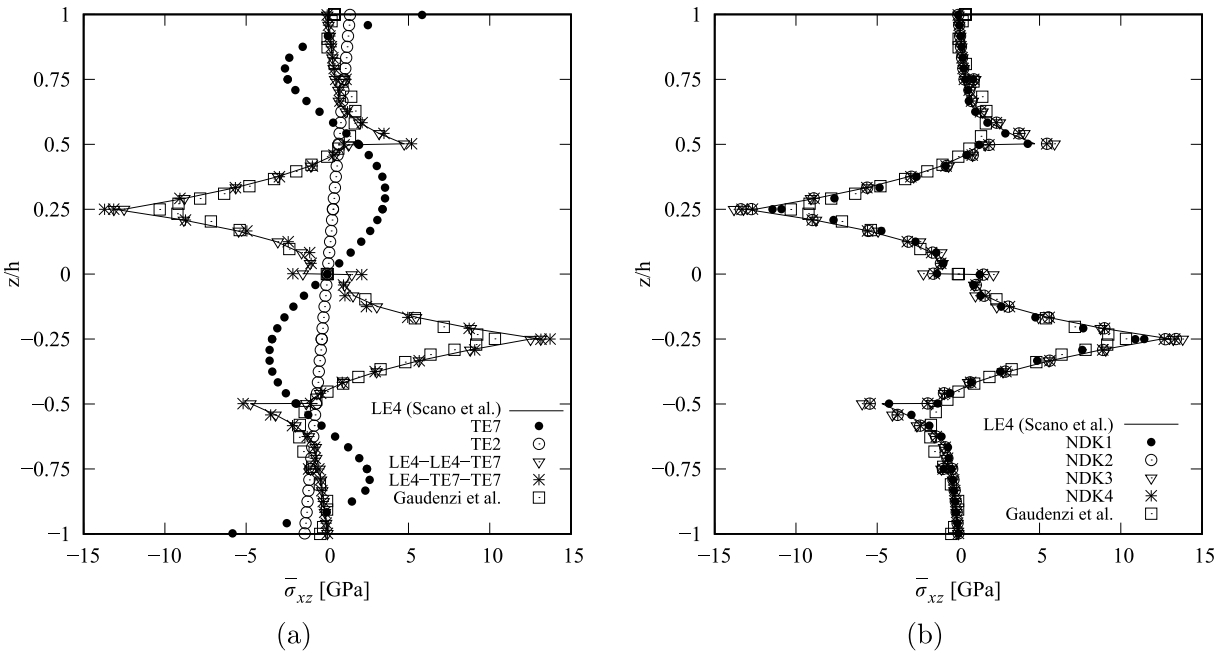


Fig. 12. Shear stresses, σ_{xz}, along z of the quasi-iso $[90°/0°/45°/-45°]_s$ laminate.

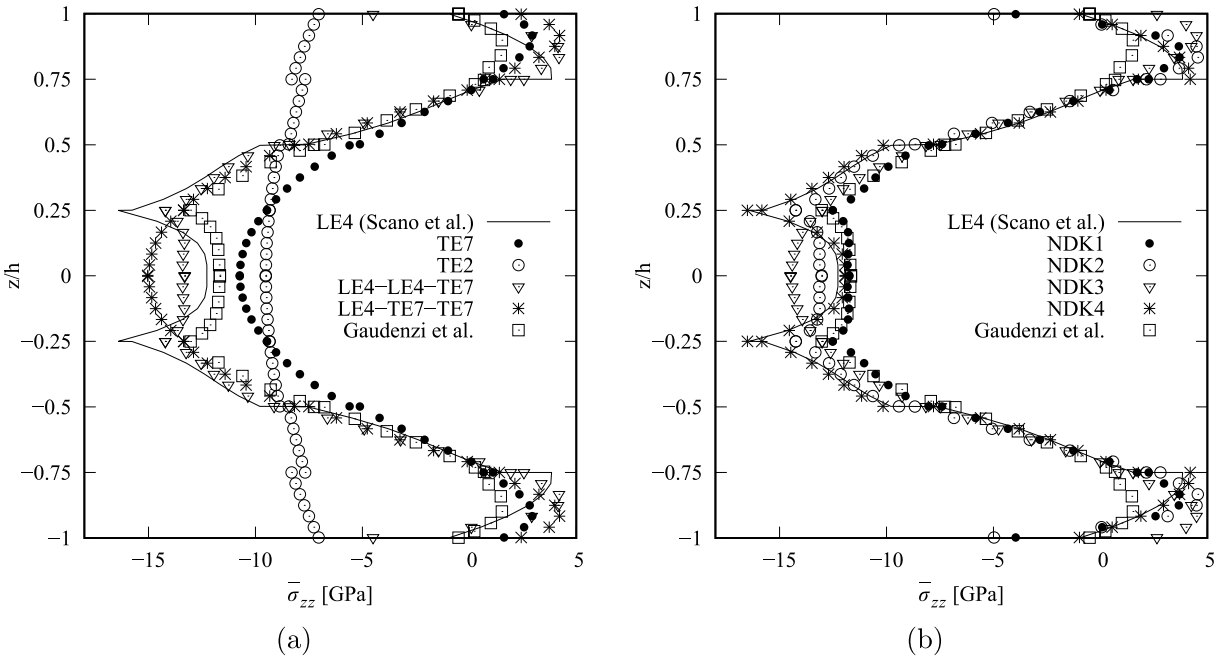


Fig. 13. Transverse stresses, σ_{zz}, along z of the quasi-iso $[90°/0°/45°/-45°]_s$ laminate.

- Model NDK4 reproduces the results of the full LE4 model, confirming its ability to obtain a high-fidelity response with optimized kinematics.

5.2. Composite plate with 32 layers

The second example investigates the free-edge stress field in a composite plate with a rectangular geometry, defined by a length L = 40 [mm], a width b = 20 [mm], and a thickness h = 8.128 [mm], as depicted in Fig. 14. Each layer has height 0.254 [mm]. The plate consists of 32 layers organized in the symmetric stacking sequence $[90°/-45°/0°/45°]_{4s}$. The composite material has the following properties: E_1 = 205 [GPa], $E_2 = E_3$ = 9.7 [GPa], $\nu_{12} = \nu_{13}$ = 0.35, ν_{23} = 0.265, $G_{12} = G_{13}$ = 4.7 [GPa] G_{23} = 3.8 [GPa]. Here, a structure characterized by a high longitudinal elastic modulus and several layers is chosen, which is representative of several aerospace applications. See for instance, Al-Mosawe et al. [74]. Similarly to the previous case, the plate is subjected to a uniform axial strain ϵ_0 along the x-axis. The analysis focuses on evaluating the transverse normal stress σ_{zz} through the thickness at a location near the free edge at $y/b = 0.998$, and along the mid-plane in the x-direction at $x = 0$. The results are compared with those from a refined three-dimensional ABAQUS model employing C3D20R elements. This reference model consists of 129,792 elements,

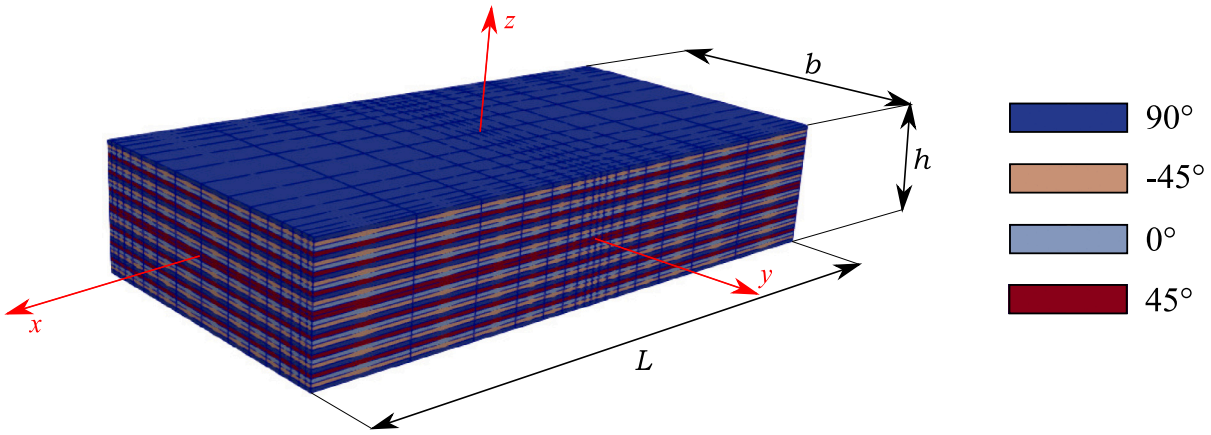


Fig. 14. Geometrical details for the 32-layered composite plate.

Table 2
Unified formulation models used for the quasi-isotropic $[90°/0°/45°/-45°]_s$ laminate.

Global model	Local model	DOF	DOF reduction [%]	Theory description
Uniform models				
LE4-LE4-LE4	LE4-LE4-LE4	81 675	–[a]	LE4 (Scano et al.)
TE7-TE7-TE7	TE7-TE7-TE7	26 136	68.00	TE7
TE2-TE2-TE2	TE2-TE2-TE2	9801	88.00	TE2
TE-LE models				
LE4-LE4-TE7	LE4-LE4-TE7	63 162	22.67	LE4-LE4-TE7
LE4-TE7-TE7	LE4-TE7-TE7	44 649	45.33	LE4-TE7-TE7
NDK models				
TE2-TE2-TE2	LE4-LE4-TE7	19 993	75.52	NDK1
TE1-TE1-TE1	LE4-LE4-TE7	17 350	78.66	NDK2
TE1-TE1-TE1	LE4-TE7-TE7	13 814	83.09	NDK3
TE1-TE1-TE1	LE4-LE4-LE4	20 866	74.45	NDK4

[a] Taken as the reference solution.

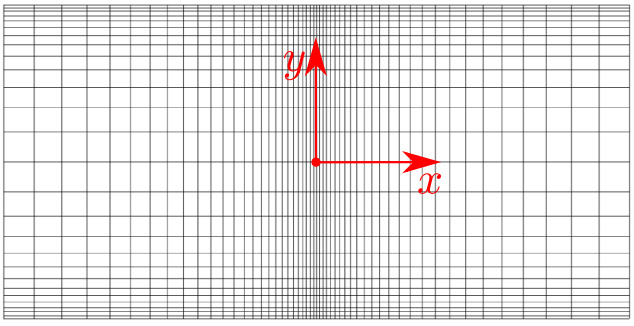


Fig. 15. In-plane mesh, 26 × 52 elements, for the ABAQUS reference model, see Table 3 for details.

with three elements used through the thickness of each material layer. The 26 × 52 in-plane mesh is illustrated in Fig. 15.

Regarding the CUF models, a single LE4 expansion is assigned to each material layer, resulting in 32 CUF elements through the thickness. For the FE discretization, the same FE mesh employed in the previous benchmark case is utilized here, namely a 16 × 16 discretization, which was found to be sufficient given the greater thickness of the 32-layer laminate. It is indeed well established that the required FEM mesh refinement is in part dictated by the length-to-thickness ratio a/h. However, in this specific case, the primary reason for adopting a highly refined mesh near the free edge is the particular importance of this region for accurately capturing the stress gradient. Table 3 summarizes

Table 3
Models used for the 32-layer $[90°/-45°/0°/45°]_{4s}$ laminate.

Global model	Local model	DOF	DOF reduction	Theory definition
26 × 52 × 96 ABAQUS C3D20R		1 638 111	–[a]	ABAQUS1
16 × 16 × 96 ABAQUS C3D20R		325 635	80.12	ABAQUS2
26 × 52 × 32 ABAQUS C3D20R		554 463	66.15	ABAQUS3
LE4-LE4-LE4	LE4-LE4-LE4	316 899	80.65	LE4
TE1-TE1-TE1	LE4-LE4-LE4	65 814	95.98	NDK1
TE1-TE1-TE1	LE4-TE7-TE7	28 790	98.24	NDK2
TE1-TE1-TE1	LE4-TE7-LE4	47 502	97.11	NDK3
TE1-TE1-TE1	TE7-LE4-LE4	47 502	97.11	NDK4
TE1-TE1-TE1	TE7-TE7-LE4	28 790	98.24	NDK5
TE1-TE1-TE1	TE7-LE4-TE7	28 790	98.24	NDK6

[a] Taken as the reference solution.

the characteristics of the Unified Formulation models for the 32-layer laminate, adhering to the same format as Table 1. ABAQUS2 adopts the same in-plane mesh as the two-dimensional plate models employed in the present work, discretizing each material layer with three solid elements through the thickness. On the contrary, ABAQUS3 employs the same in-plane mesh as the ABAQUS reference model, with a single solid element assigned to each material layer.

In the present work, the analyses are carried out exclusively using classical solid elements. It is acknowledged, however, that commercial finite element codes offer more advanced modelling strategies, such as submodelling and substructuring techniques, which could be employed to reduce the total number of degrees of freedom. The application of such approaches would necessitate a thorough discussion on the appropriate size of the local region required for an accurate representation of the boundary layer phenomenon. In the following papers, it would be interesting to compare the proposed formulation with such techniques. Thus, the degrees of freedom reported in Table 3 should be regarded as representative upper-bound values.

Furthermore, two less refined ABAQUS models are compared to illustrate that a very refined solid model is needed to obtain reliable results. The DOF reduction is described as follows:

$$\text{DOF Reduction} = \left\| \frac{\text{DOF (ABAQUS1)} - \text{DOF (Theory)}}{\text{DOF (ABAQUS1)}} \right\| \times 100 \tag{28}$$

The distributions of the transverse normal stress σ_{zz} are presented in Figs. 16 and 17. The first graph presents results for models where the refined local zone employs the LW LE4 expansion for the in-plane displacement component u_x. Conversely, the second plot shows results where the refined zone consistently uses the TE7 expansion for u_x. Due to the symmetry of the problem, only the upper half of the thickness is displayed.

Based on the preceding analyses, the following conclusions can be drawn:

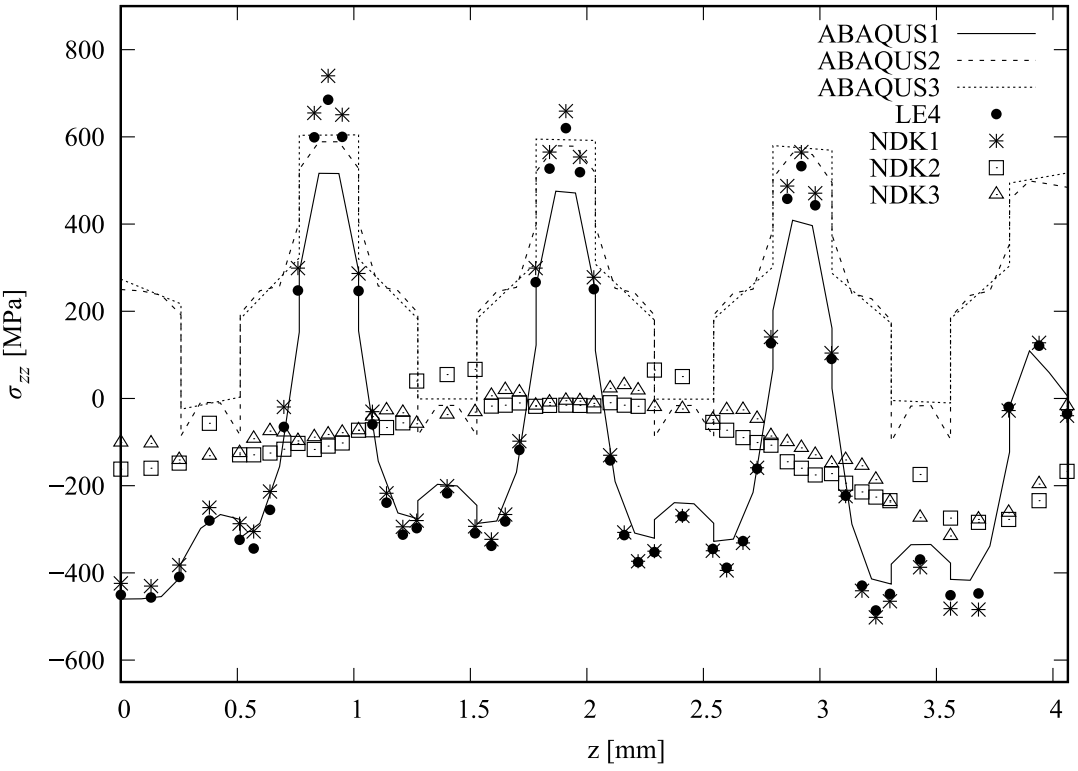


Fig. 16. Transverse stresses, σ_{zz}, along z of the 32-layer $[90°/-45°/0°/45°]_{4s}$ laminate when u_x adopts the LW approach.

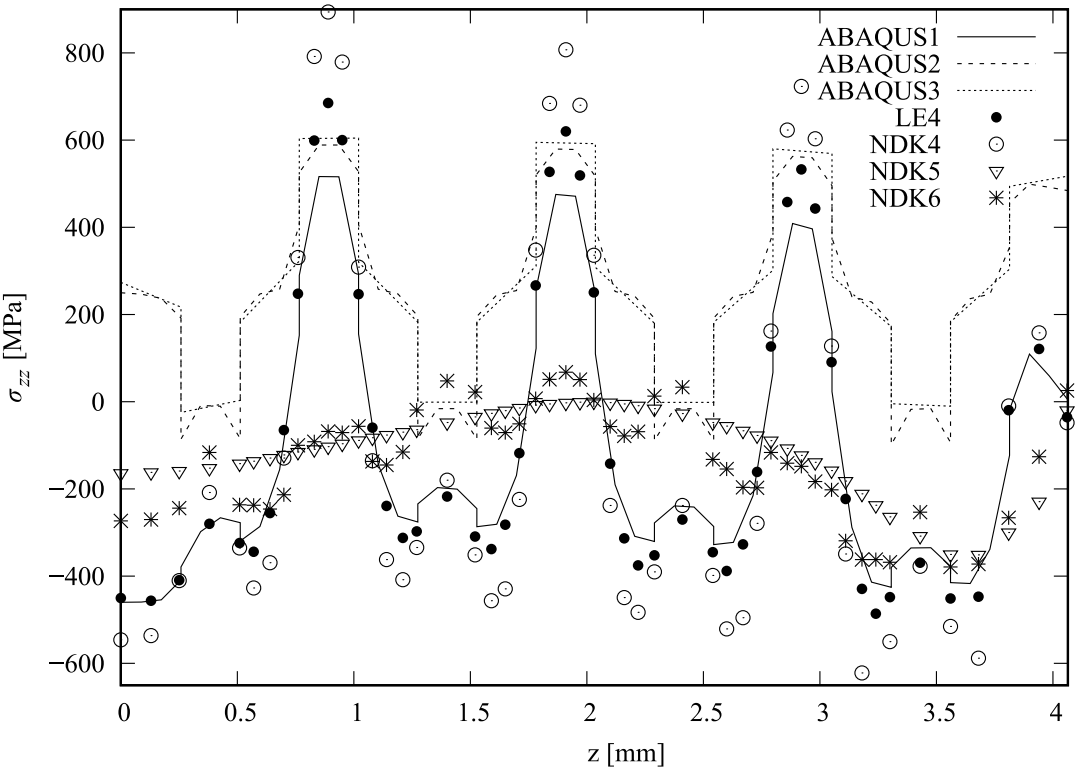


Fig. 17. Transverse stresses, σ_{zz}, along z of the 32-layer $[90°/-45°/0°/45°]_{4s}$ laminate when u_x adopts the ESL approach.

- The proposed CUF models demonstrate significantly higher computational efficiency compared to a refined three-dimensional ABAQUS reference model.
- Consistent with previous findings, accurate prediction of interlaminar stresses necessitates the use of higher-order LW kinematics only in the vicinity of the free edge. The results show that the peaks arise at the −45°-90° interface.
- For the calculation of σ_{zz}, the u_z displacement component is critical. Models NDK2 and NDK3 do not provide adequate results for this stress component. In contrast, the NDK4 model shows that both the u_y and u_z displacement components are essential to accurately capture the stress trend, yielding results comparable to the reference solution and the complete LE4 model.

6. Conclusions

This work introduces an enhanced method for the two-dimensional analysis of structures within the CUF framework. The method reformulates the classical CUF approach and reorganizes the assembly procedure of the FE matrices. It is built upon two fundamental innovations that were independently proposed in previous works: (1) the ability to assign different expansion types, specifically Taylor- and Lagrange-based expansions, to each displacement variable, and (2) the incorporation of Node-Dependent Kinematics (NDK), which allows the use of a distinct kinematic model per each finite element node. Thus, the presented method permits to have a greater degree of practical flexibility with respect to previously presented formulations.

The numerical analyses performed lead in the present work to the following conclusions:

- The proposed method successfully combines different expansion types and polynomial orders, enabling a significant reduction in degrees of freedom through a targeted selection of kinematics at each node.
- It facilitates local kinematic refinements without modifying the underlying finite element mesh. In fact, it is possible to use lower-order theories in a large zone of the plate, while using very refined theories in a limited region.
- The optimal selection of models depends on both the specific output quantity of interest and the type of problem being analysed. In such cases, the accurate computation of the transverse normal stress demands kinematic models of greater refinement than those required for the shear stress components.
- The proposed examples demonstrate the capabilities to study different types of stacking sequences.
- The results show that the proposed global/local models clearly identify gradients of the stress field as the free edge is approached.
- The more refined NDK models are able to satisfy the traction-free condition for both shear and transverse stresses.
- With regard to the quasi-isotropic properties of the last two benchmarks, it is instructive to consider the ABD matrix, in particular, the condition $A_{11} = A_{22}$, that characterizes the in-plane response of the laminate as globally isotropic. Nevertheless, the free-edge effect is a localized phenomenon that is primarily governed by the anisotropy along the thickness direction, rendering the accurate evaluation of transverse stress components particularly important.

Future work will focus on extending this methodology to shell formulations and multi-physics problems. Also, other types of expansions will be studied, such as the use of the Legendre polynomials.

CRediT authorship contribution statement

Erasmo Carrera: Writing – review & editing, Supervision, Resources, Methodology, Funding acquisition, Conceptualization. **Daniele Scano:** Writing – original draft, Visualization, Validation, Software, Methodology, Investigation, Formal analysis, Data curation, Conceptualization. **Enrico Zappino:** Writing – review & editing, Visualization, Supervision, Software, Resources, Methodology, Funding acquisition, Conceptualization.

Declaration of competing interest

The authors declare that they have no known competing financial interests or personal relationships that could have appeared to influence the work reported in this paper.

Data availability

Data will be made available on request.

References

[1] Reddy JN, Robbins Jr DH. Theories and computational models for composite laminates. Appl Mech Rev 1994;47(6):147–69.
[2] Mittelstedt C, Becker W. Interlaminar stress concentrations in layered structures: Part I - a selective literature survey on the free-edge effect since 1967. J Compos Mater 2004;38(12):1037–62.
[3] Carrera E. Developments, ideas, and evaluations based upon Reissner's Mixed Variational Theorem in the modeling of multilayered plates and shells. Appl Mech Rev 2001;54(4):301–29.
[4] Kirchhoff G. Über das gleichgewicht und die bewegung einer elastischen scheibe. J Für Die Reine Und Angew Math (Crelles Journal) 1850;1850(40):51–88.
[5] Love AEH. a treatise on the mathematical theory of elasticity. Cambridge University Press; 1927.
[6] Reissner E, Stavsky Y. Bending and stretching of certain types of heterogeneous aeolotropic elastic plates. J Appl Mech 1961;28:402–8.
[7] Reissner E. The effect of transverse shear deformation on the bending of elastic plates. J Appl Mech 1945;12:69–77.
[8] Mindlin R. Influence of rotary inertia and shear flexural motion of isotropic, elastic plates. J Appl Mech 1951;18:31–8.
[9] Reddy JN. Mechanics of laminated composite plates and shells: theory and analysis. New York, USA: CRC Press; 1997.
[10] Palazotto AN, Dennis ST. Nonlinear analysis of shell structures. AIAA Ser 1992.
[11] Kant T, Manjunatha BS. An unsymmetric frc laminate c° finite element model with 12 degrees of freedom per node. Eng Comput 1988;5(4):300–8.
[12] Reddy JN. A simple higher-order theory for laminated composite plates. J Appl Mech 1984;51:745–52.
[13] Senthilnathan NR, Lim SP, Lee KH, Chow ST. Buckling of shear-deformable plates. AIAA J 1987;25(9):1268–71.
[14] Maji A, Mahato PK. Development and applications of shear deformation theories for laminated composite plates: An overview. J Thermoplast Compos Mater 2022;35(12):2576–619.
[15] Carrera E, Cinefra M, Zappino E, Petrolo M. finite element analysis of structures through unified formulation. Chichester, United Kingdom: John Wiley & Sons Ltd; 2014.
[16] Carrera Erasmo. Single vs multilayer plate modelings on the basis of reissner's mixed theorem. AIAA J 2000;38(342–352):02.
[17] Demasi L. ∞^3 hierarchy plate theories for thick and thin composite plates: The generalized unified formulation. Compos Struct 2008;84(3):256–70.
[18] Demasi L. Partially Zig-Zag Advanced Higher Order Shear Deformation Theories Based on the Generalized Unified Formulation. Compos Struct 2012;94(2):363–75.
[19] Demasi L, Ashenafi Y, Cavallaro R, Santarpia E. Generalized unified formulation shell element for functionally graded variable-stiffness composite laminates and aeroelastic applications. Compos Struct 2015;131:501–15.
[20] Carrera E, Scano D, Zappino E. Plate finite elements with arbitrary displacement fields along the thickness. Finite Elem Anal Des 2025;244:104296.
[21] Scano D, Carrera E, Zappino E. Shell finite elements with arbitrary displacement fields along the thickness. Int J Solids Struct 2025;321:113544.
[22] Petrolo M, Carrera E. Best theory diagrams for multilayered structures via shell finite elements. Adv Model Simul Eng Sci 2019;6(4):1.
[23] Carrera E, Scano D, Petrolo M. Evaluation of variable kinematics beam, plate, and shell theories using the asymptotic-axiomatic method. Mech Solids 2025;60(1):311–37.

[24] Carrera E. A class of two-dimensional theories for anisotropic multilayered plates analysis. In: Atti della accademia delle scienze di torino. classe di scienze fisiche matematiche e naturali. 1995, 19–20:1–39.
[25] Carrera E, Campisi C, Cinefra M, Soave M. Evaluation of various theories of the thickness and curvature approximations for free vibrational analysis of cylindrical and spherical shells. Int J Veh Noise Vib 2011;7(1):16–36.
[26] Carrera E. Theories and finite elements for multilayered plates and shells: a unified compact formulation with numerical assessment and benchmarking. Arch Comput Methods Eng 2003;10(3):215–96.
[27] Petrolo M, Iannotti P. Best theory diagrams for laminated composite shells based on failure indexes. Aerotec Missili & Spaz 2023;102:199–218.
[28] Petrolo M, Augello R, Carrera E, Scano D, Pagani A. Evaluation of transverse shear stresses in layered beams/plates/shells via stress recovery accounting for various CUF-based theories. Compos Struct 2023;307:116625.
[29] Pagani A, Carrera E, Augello R, Scano D. Use of Lagrange polynomials to build refined theories for laminated beams, plates and shells. Compos Struct 2021;276:114505.
[30] Hayashi T. Analytical study of interlaminar shear stresses in a laminated composite plate. Trans Jpn Soc Aeronaut Space Sci 1967;10(17):43–8.
[31] Puppo AH, Evensen HA. Interlaminar shear in laminated composites under generalized plane stress. J Compos Mater 1970;4(2):204–20.
[32] Pipes RB, Pagano NJ. Interlaminar stresses in composite laminates under uniform axial extension. J Compos Mater 1970;4(4):538–48.
[33] Pipes RB, Pagano NJ. Interlaminar Stresses in Composite Laminates–An Approximate Elasticity Solution. J Appl Mech 1974;41(3):668–72.
[34] Pagano NJ. On the Calculation of Interlaminar Normal Stress in Composite Laminate. J Compos Mater 1974;8(1):65–81.
[35] Whitney JM, Sun CT. A higher order theory for extensional motion of laminated composites. J Sound Vib 1973;30(1):85–97.
[36] Wang ASD, Crossman FW. Some New Results on Edge Effect in Symmetric Composite Laminates. J Compos Mater 1977;11(1):92–106.
[37] Whitcomb JD, Raju IS, Goree JG. Reliability of the finite element method for calculating free edge stresses in composite laminates. Comput Struct 1982;15(1):23–37.
[38] Raju IS, Crews JH. Interlaminar stress singularities at a straight free edge in composite laminates. Comput Struct 1981;14(1):21–8.
[39] Robbins Jr DH, Reddy JN. Modelling of thick composites using a layerwise laminate theory. Internat J Numer Methods Engrg 1993;36(4):655–77.
[40] Vidal P, Gallimard L, Polit O. Assessment of variable separation for finite element modeling of free edge effect for composite plates. Compos Struct 2015;123:19–29.
[41] Wang SS, Choi I. Boundary-layer effects in composite laminates: Part 1–Free-edge stress singularities. J Appl Mech 1982;49(3):541–8.
[42] Daví G, Milazzo A. Boundary element solution for free edge stresses in composite laminates. J Appl Mech 1997;64(4):877–84.
[43] Mittelstedt C, Becker W. Efficient computation of order and mode of three-dimensional stress singularities in linear elasticity by the boundary finite element method. Int J Solids Struct 2006;43(10):2868–903.
[44] Dölling S, Hahn J, Felger J, Bremm S, Becker W. A scaled boundary finite element method model for interlaminar failure in composite laminates. Compos Struct 2020;241:111865.
[45] Mittelstedt Christian, Becker Wilfried, Kappel Andreas, Kharghani Navid. Free-edge effects in composite laminates–A review of recent developments 2005–2020. Appl Mech Rev 2022;74(1):010801.
[46] de Miguel AG, Pagani A, Carrera E. Free-edge stress fields in generic laminated composites via higher-order kinematics. Compos Part B: Eng 2019;168:375–86.
[47] de Miguel AG, Kaleel I, Nagaraj MH, Pagani A, Petrolo M, Carrera E. Accurate evaluation of failure indices of composite layered structures via various fe models. Compos Sci Technol 2018;167:174–89.
[48] D'Ottavio M, Vidal P, Valot E, Polit O. Assessment of plate theories for free-edge effects. Compos Part B: Eng 2013;48:111–21.
[49] Stapleton SE, Stier B, Jones S, Bergan A, Kaleel I, Petrolo M, Carrera E, Bednarcyk BA. A critical assessment of design tools for stress analysis of adhesively bonded double lap joints. Mech Adv Mater Struct 2021;28(8):791–811.
[50] Scano D, Carrera E, Petrolo M. Use of the 3D equilibrium equations in the free-edge analyses for laminated structures with the variable kinematics approach. Aerotec Missili & Spaz 2024;103:179–95.
[51] Airoldi A, Baldi A, Bettini P, Sala G. Efficient modelling of forces and local strain evolution during delamination of composite laminates. Compos Part B: Eng 2015;72:137–49.
[52] Noor AK. Global-local methodologies and their application to nonlinear analysis. Finite Elem Anal Des 1986;2(4):333–46.
[53] Fish J, Pan L, Belsky V, Gomaa S. Unstructured multigrid method for shells. Internat J Numer Methods Engrg 1996;39(7):1181–97.
[54] Prager W. Variational principles for elastic plates with relaxed continuity requirements. Int J Solids Struct 1968;4(9):837–44.
[55] Park KC, Felippa CA. A variational principle for the formulation of partitioned structural systems. Internat J Numer Methods Engrg 2000;47(1–3):395–418.
[56] Aminpour MA, Ransom JB, McCleary SL. A coupled analysis method for structures with independently modelled finite element subdomains. Internat J Numer Methods Engrg 1995;38(21):3695–718.
[57] Ransom JB. On multifunctional collaborative methods in engineering science. National Aeronautics and Space Administration, Langley Research Center; 2001.
[58] Brezzi F, Marini LD. The three-field formulation for elasticity problems. GAMM-Mitt 2005;28(2):124–53.
[59] Blanco PJ, Feijóo RA, Urquiza SA. A variational approach for coupling kinematically incompatible structural models. Comput Methods Appl Mech Engrg 2008;197(17):1577–602.
[60] Blanco P, Gervasio P, Quarteroni A. Extended variational formulation for heterogeneous partial differential equations. Comput Methods Appl Math 2011;11(2):141–72.
[61] Dhia BH. Problèmes mécaniques multi-échelles: la méthode arlequin. Comptes Rendus de L'Académie Des Sci - Ser IIB - Mechanics-Physics-Astronomy 1998;326(12):899–904.
[62] Dhia HB, Rateau G. The arlequin method as a flexible engineering design tool. Internat J Numer Methods Engrg 2005;62(11):1442–62.
[63] Biscani F, Giunta G, Belouettar S, Carrera E, Hu H. Variable kinematic plate elements coupled via arlequin method. Internat J Numer Methods Engrg 2012;91(12):1264–90.
[64] Biscani F, Nali P, Belouettar S, Carrera E. Coupling of hierarchical piezoelectric plate finite elements via arlequin method. J Intell Mater Syst Struct 2012;23(7):749–64.
[65] Zappino E, Li G, Pagani A, Carrera E. Global-local analysis of laminated plates by node-dependent kinematic finite elements with variable esl/lw capabilities. Compos Struct 2017;172:1–14.
[66] Carrera E, Valvano S, Kulikov M. Electro-mechanical analysis of composite and sandwich multilayered structures by shell elements with node-dependent kinematics. Int J Smart Nano Mater 2018;9(1):1–33.
[67] Nagaraj MH, Carrera E, Petrolo M. A global–local approach to the high-fidelity impact analysis of composite structures based on node-dependent kinematics. Compos Struct 2023;304:116307.
[68] Zappino E, Carrera E. Global-local multi-field models for the stress analysis of laminated structures. Philos Trans R Soc A: Math Phys Eng Sci 2022;381(2240):20210218.
[69] Carrera E, Zappino E. One-dimensional finite element formulation with node-dependent kinematics. Comput Struct 2017;192:114–25.
[70] Carrera E, Scano D. Beam finite element models with node dependent kinematics and arbitrary displacement fields over the cross-section. Mech Adv Mater Struct 2025;1–14.
[71] Washizu K. Variational methods in elasticity and plasticity. Oxford, United Kingdom: Pergamon; 1968.
[72] Bathe KJ. Finite element procedure. Upper Saddle River, New Jersey, USA: Prentice hall; 1996.
[73] Gaudenzi P, Mannini A, Carbonaro R. Multi-layer higher-order finite elements for the analysis of free-edge stresses in composite laminates. Internat J Numer Methods Engrg 1998;41(5):851–73.
[74] Al-Mosawe A, Al-Mahaidi R, Zhao X-L. Engineering properties of CFRP laminate under high strain rates. Compos Struct 2017;180:9–15.